General Disclaimer

One or more of the Following Statements may affect this Document

- This document has been reproduced from the best copy furnished by the organizational source. It is being released in the interest of making available as much information as possible.

- This document may contain data, which exceeds the sheet parameters. It was furnished in this condition by the organizational source and is the best copy available.

- This document may contain tone-on-tone or color graphs, charts and/or pictures, which have been reproduced in black and white.

- This document is paginated as submitted by the original source.

- Portions of this document are not fully legible due to the historical nature of some of the material. However, it is the best reproduction available from the original submission.

ASA/C-43205-C/FR/75

Final Report

Research for Preparation of Cation-Conducting Solids by High-Pressure Synthesis and Other Methods

31 March 1975

Lincoln Laboratory

MASSACHUSETTS INSTITUTE OF TECHNOLOGY

LEXINGTON, MASSACHUSETTS

MASSACHUSETTS INSTITUTE OF TECHNOLOGY

Lincoln Laboratory

RESEARCH FOR PREPARATION OF CATION-CONDUCTING SOLIDS BY HIGH-PRESSURE SYNTHESIS AND OTHER METHODS

Final Report

1 August 1973 – 28 February 1975

SUMMARY

We have shown that two body-centered-cubic skeleton structures, the Im3 $KSbO_3$ phase and the defect-pyrochlore phase $A^+B_2X_6$, do exhibit fast Na^+-ion transport. Moreover, we have shown that placement of anions at the tunnel-intersection sites does not impede Na^+-ion transport in $NaSbO_3 \cdot \frac{1}{6} NaF$, and may not in $Na_{1+2x}Ta_2O_5F \cdot O_x$. However, the activation energies $\epsilon_a \approx 0.35$ eV are higher than those found in β-alumina. There are two possible explanations for the higher ϵ_a: (1) breathing of the "bottleneck" (site face or edge) through which the A^+ ions must pass on jumping from one site to another may be easier in a layer structure, and/or (2) A^+-O bonding may be stronger in the cubic structures because the O^{2-} ion bonds with two (instead of three) cations of the skeleton. If the former explanation is dominant, a lower ϵ_a may be achieved by optimizing the lattice parameter. If the latter is dominant, a new structural principle may have to be explored.

PRECEDING PAGE BLANK NOT FILME

I. GOALS AND STRATEGY

A practical Na-S cell would provide an energy density of $\sim$ 100 Wh/lb. Mobile energy storage of this density would have a variety of important applications.

Two critical components of the Na-S cell are: (1) a suitable positive electrode and (2) a durable solid-electrolyte membrane that transports Na^+ ions with a low resistivity at a practical operating temperature. This study addressed itself to the solid electrolyte.

The discovery[1] that β-alumina, $(Na_2O)_{1+x} \cdot 11Al_2O_3$, has a resistivity for Na^+-ion transport at 300^oC of $\rho_{300} \approx 5\,\Omega$ cm first alerted the technical community to the possibility of realizing a practical Na-S cell. Initial problems with ceramic fabrication and with breakdown of the membrane on cell charging motivated a search for other solid-electrolyte materials. The object of the search was a material having Na^+-ion transport superior to that of the best β''-alumina: i.e. $\rho_{300} \sim 4\,\Omega$ cm and an activation energy $\epsilon_a < 0.16$ eV.

Both β''- and β-alumina consist of Na_2O layers between spinel blocks of γ-Al_2O_3. This type of structure has two disadvantages: (1) an anisotropic thermal expansion[2] and (2) two-dimensional Na^+-ion conduction in only a small fraction of the material. Although one-dimensional tunnel structures appear promising, they suffer from blockage by impurities, defects, or grain boundaries. It seemed to us more promising to explore cubic "skeleton" structures.

A skeleton structure consists of a rigid subarray with intersecting channels, or tunnels, in which alkali ions can move in three dimensions. Our strategy was to investigate, first, the Im3 phase of high-pressure $KSbO_3$ to determine whether the concept was valid. We succeeded in fabricating $NaSbO_3$ and $NaSbO_3 \cdot \frac{1}{6} NaF$ disks of ca 95 percent theoretical density, and we measured a Na^+-ion resistivity at 300^oC of $\rho_{300} \approx 13\,\Omega$ cm with an activation energy $\epsilon_a \approx 0.35$ eV. These results demonstrated the validity of the concept, even though the activation energy was a factor two too high.

No attempt was made to optimize the tunnel size in this structure because the long-life chemical stability of the compound in contact with molten sodium seemed dubious. Therefore, we decided to turn to other skeleton structures.

Dr. Joseph Singer of NASA suggested to us that the defect pyrochlores $A^+B_2X_6$ were candidate skeleton structures. Initial measurements on $Na(TaW)O_6$ proved promising. Since W^{6+} ions are not stable in the presence of molten sodium, we decided to investigate intensively the compound $NaTa_2O_5F$. A number of chemical problems arose in the course of these studies.

Some attention was also given to aluminosilicates having the $(AlSiO_4)^-$ skeleton of carnegieite. Although moderately good ionic conductors, they did not appear as promising as the defect pyrochlores.

II. DESCRIPTION OF THE STRUCTURES

A. The Im3 Phase

A primitive-cubic Pn3 phase of $KSbO_3$ was first discovered by Spiegelberg.[3] The structure is composed of an $(SbO_3)^-$ subarray skeleton, as shown in Fig. 1, and an ordered arrangement of K^+ ions within $\langle 111 \rangle$ tunnels that traverse the skeleton, intersecting at the origin (center of front face in Fig. 1) and body-center positions. The $(SbO_3)^-$ network is built up of pairs of edge-shared SbO_6 octahedra, forming Sb_2O_{10} clusters, that are connected by shared corners. The $\langle 111 \rangle$ tunnels are made up of face-shared octahedral sites that are compressed along the tunnel axis so as to provide a large spacing between the bridging oxygens within a shared face. The intersection sites at the origin and body-center positions are large octahedral interstices, and along any $\langle 111 \rangle$ axis three octahedral sites separate an origin and body-center position. Each of the shared faces along the tunnels consists of either O_1 or O_2 oxygen atoms. The order of the faces is O_1-O_2-O_2-O_1 (see Fig. 2) and the triangular area of an O_1 face is somewhat larger than that of an O_2 face. Octahedral sites having O_1 and O_2 faces are labeled M_1 sites, those with only O_2 faces are M_2 sites. The unit cell contains $K_{12}Sb_{12}O_{36}$, the K^+ ions occupying the M_1 and M_2 positions in an ordered
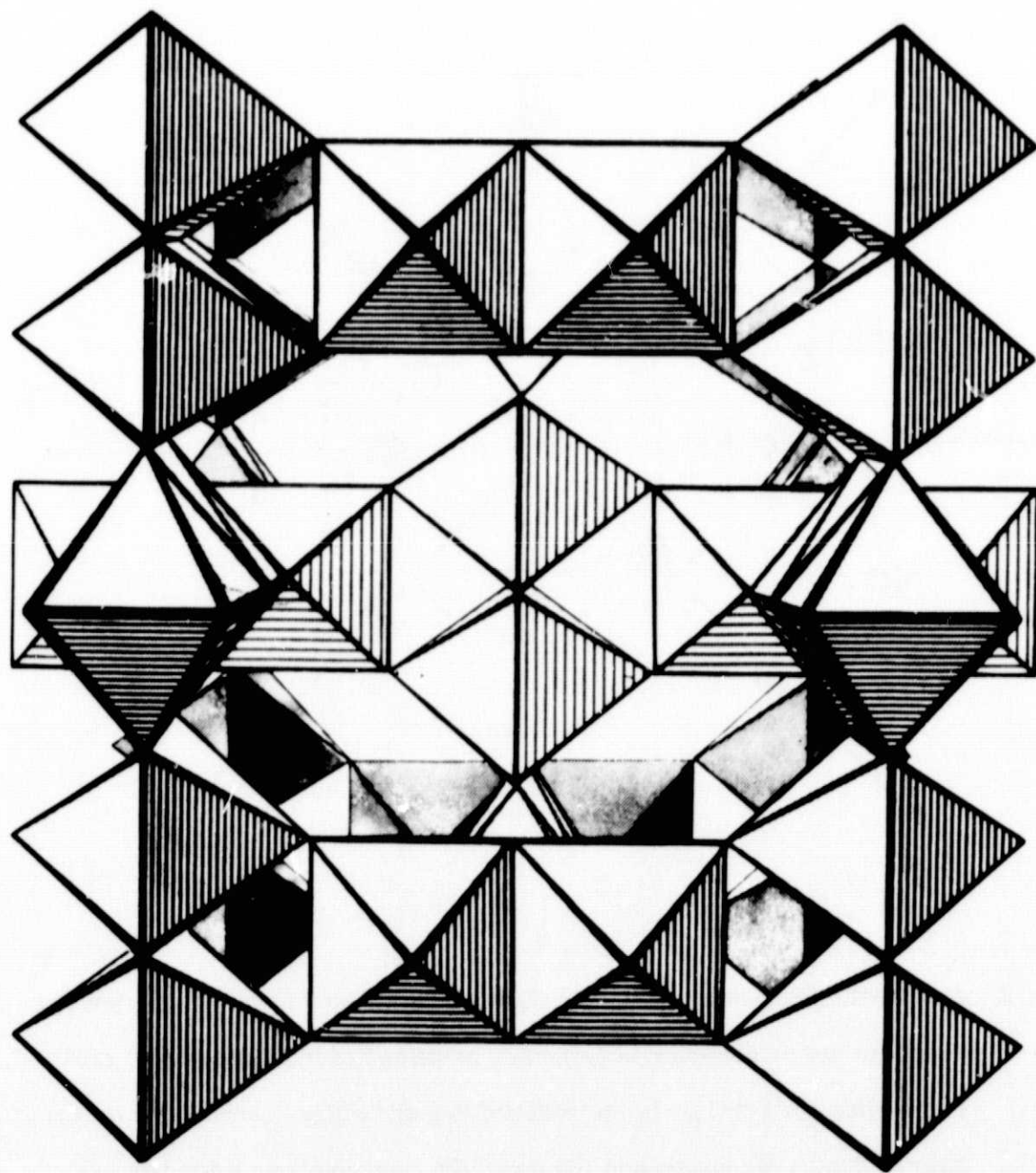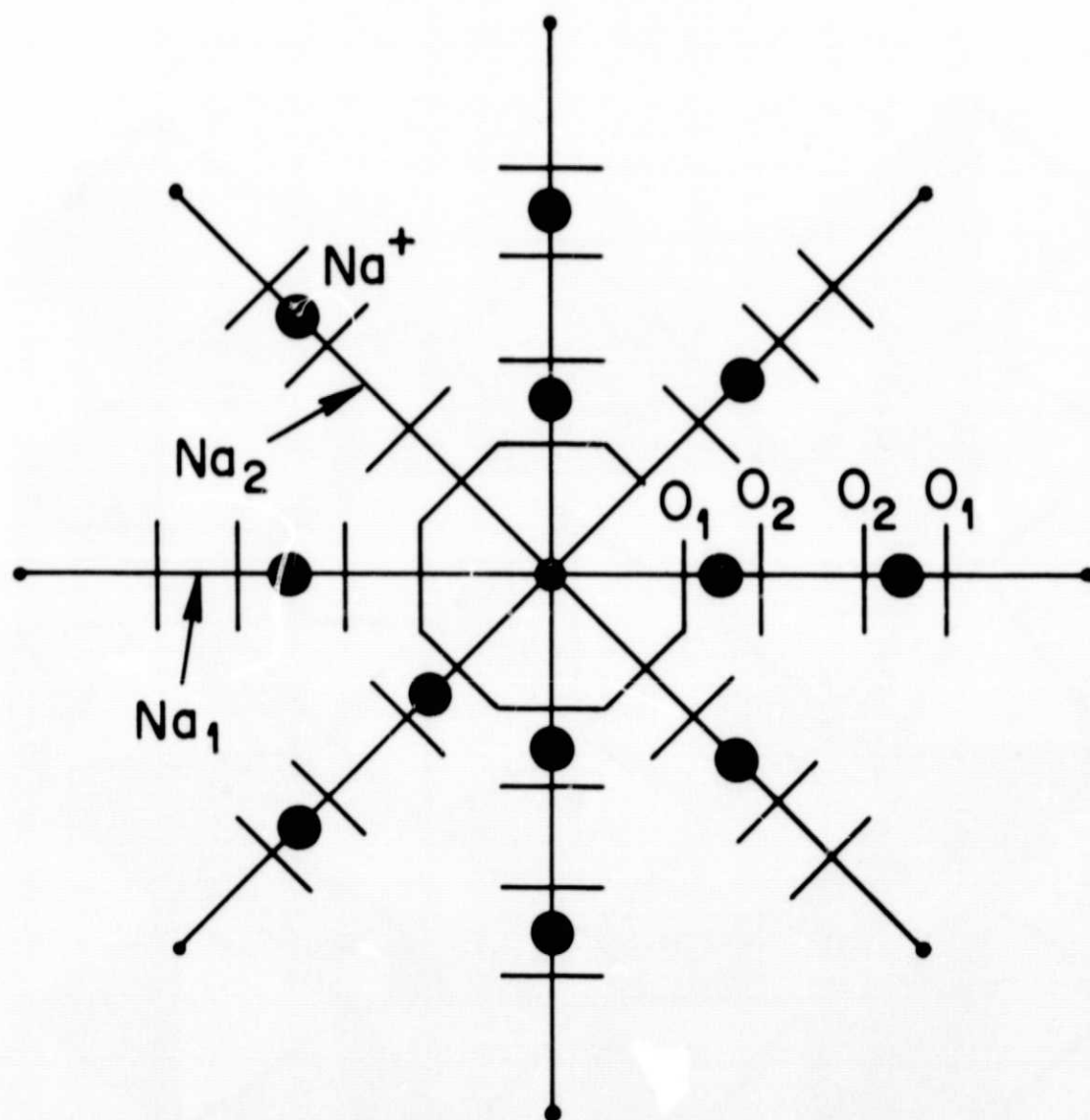
Fig. 1. The SbO$_3$ subarray of cubic KSbO$_3$.

3

Fig. 2. Schematic representation of the eight ⟨111⟩ channels branching from the origin to the neighboring body-center positions in the disordered, cubic (Im3) phase of $KSbO_3$. In the ordered Pn3 structure, each singly occupied branch has an M_2 cation and the three nearest-neighbor branches are doubly occupied.

4

manner so that each tunnel segment contains either two M_1 cations or one M_2 cation, and an M_2 cation has only M_1-cation nearest neighbors.

The stoichiometric, atmospheric-pressure phase of $KSbO_3$ has the rhombohedral ilmenite structure. During an investigation of the structural relationships among several $A^+B^{5+}O_3$ compounds, we[4] found a cubic high-pressure phase with space group Im3. This Im3 phase is similar to the primitive-cubic Pn3 phase discovered by Spiegelberg; but it contains K^+ ions randomly distributed among the M_1 and M_2 positions.

B. The Defect-Pyrochlore Structure

The cubic pyrochlore structure corresponds to the chemical formula $A_2B_2X_6X'$, where A is a large cation and B is a smaller cation octahedrally coordinated by six X anions. The B_2X_6 subarray forms a skeleton of corner-shared octahedra (see Fig. 3). Each X' anion is tetrahedrally coordinated by four A cations, and each A cation has two nearest-neighbors forming a puckered ring perpendicular to the X'-A-X' axis. With space group Fd3m and the origin chosen at a B site, the A and X' positions are identified as 16d and 8b, the cubic unit cell containing $A_{16}B_{16}X_{48}X'_8$. (The B and X positions are the 16c and 48f positions of the space group.)

Babel et al.[5] prepared a number of fluorides $A^+B^{2+}B'^{3+}F_6$, where A = Cs, Rb, or K. These fluorides have a $B^{2+}B'^{3+}F_6$ skeleton identical to the B_2X_6 pyrochlore skeleton, the B and B' atoms being randomly distributed. In place of the A_2X' subarray of a pyrochlore, only the 8b positions are occupied by a large A^+ cation. Singer[6] suggested to us that these defect pyrochlores might represent cubic skeleton structures of the type we wished to investigate. We recognized that this suggestion would be valid provided vacancies could be established on the 8b sites either by stabilizing $A^+_{1-x}B^{2+}_{1-x}B'^{3+}_{1+x}F_6$ compounds with the same structure or by obtaining the phase with a lattice parameter conducive to random occupancy of 8b and 16d positions.
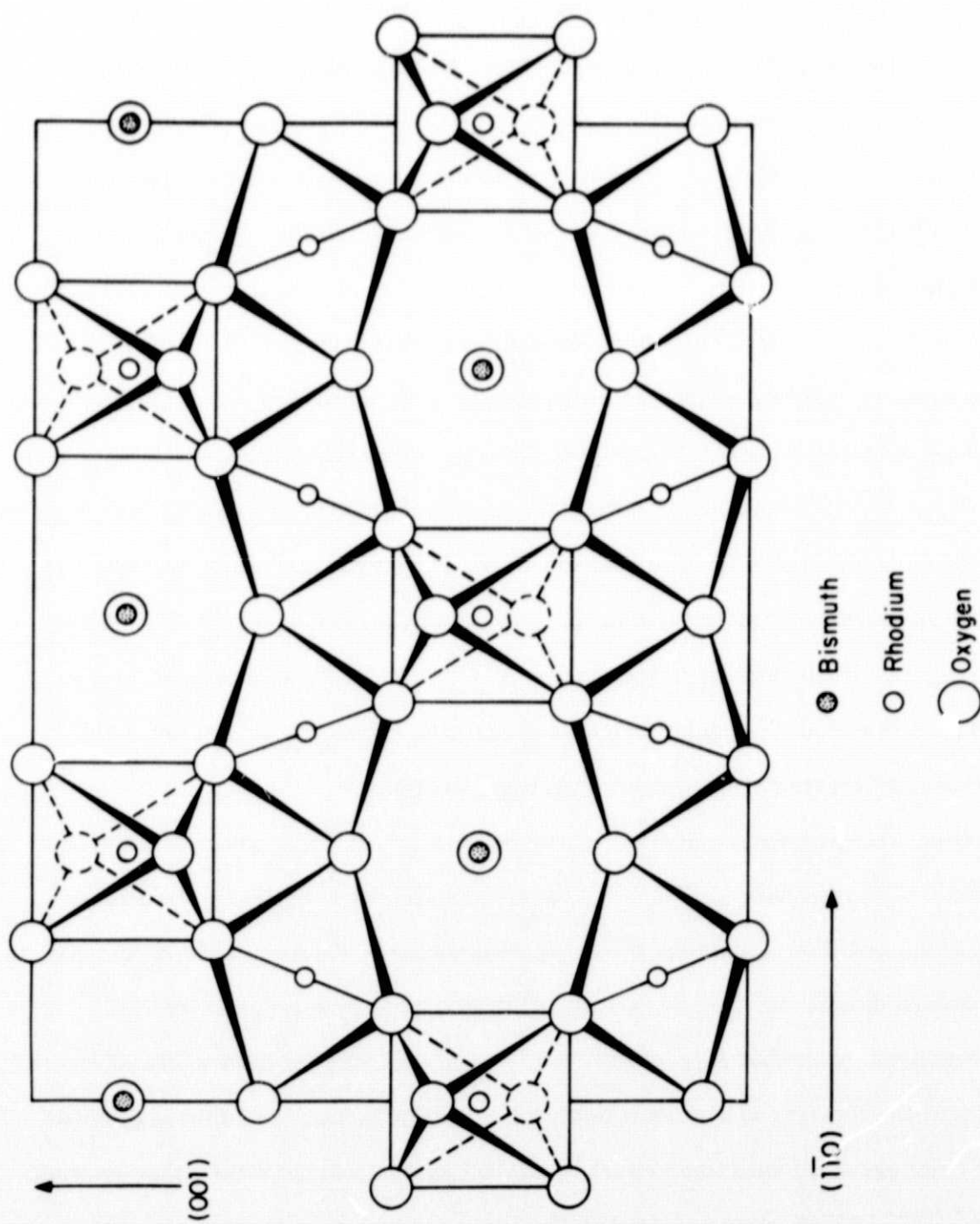
5

Fig. 3. The (110) projection of a cubic pyrochlore $Bi_2Rh_2O_7$, showing the B_2X_6 skeleton of corner-shared octahedra.

Bismuth
Rhodium
Oxygen

(001)

($1\bar{1}0$)

6

C. Carnegieites

The aluminosilicates are classic skeleton structures. The zeolites, for example, form molecular sieves. As these latter structures are stabilized by water, they are unsuitable for solid electrolytes that are to be in contact with molten alkali metal. Moreover, the openings are too large for optimal alkali-ion transport. The high-temperature form of $NaAlSiO_4$, carnegieite , is a more interesting possibility.

Carnegieite has a cubic $(AlSiO_4)^-$ skeleton having the structure of cubic SiO_2 (see Fig. 4). In the idealized structure, the Al and Si atoms form a cubic zincblende array with oxygen atoms on every Al-Si bond axis. This arrangement provides a network of corner-shared tetrahedra that, in the real carnegieite structure, becomes distorted to a primitive-cubic array by interaction with the Na^+ ions in the large voids about the body-center and edge-center positions. Note that, in the idealized structure, the O^{2-}-ion array is half as dense as a cubic-close-packed array. It can be derived from the close-packed array by removal of alternate $[110]$ or $[1\bar{1}0]$ rows.

III. SAMPLE PREPARATION

A. Hot-Pressed Ceramic Disks

Transport measurements are made on dense, polycrystalline ceramic disks approximately 1/2" in diameter and 0.05" to 0.1" thick. Densities in excess of 90 percent, and preferably 95 percent, of theoretical are required for proper material evaluation.

There is no general method for obtaining disks of very high density. The method chosen in each case depends necessarily on the properties of the particular material. Some of the more important properties that must be considered are stability and particle size:

1. Thermal stability. If a material can be heated to temperatures near the melting point $(T/T_{melt} > 0.75)$, high densities in be achieved even without pressure. If high temperatures cannot be used to achieve densification, high pressure and/or a flux may be required.
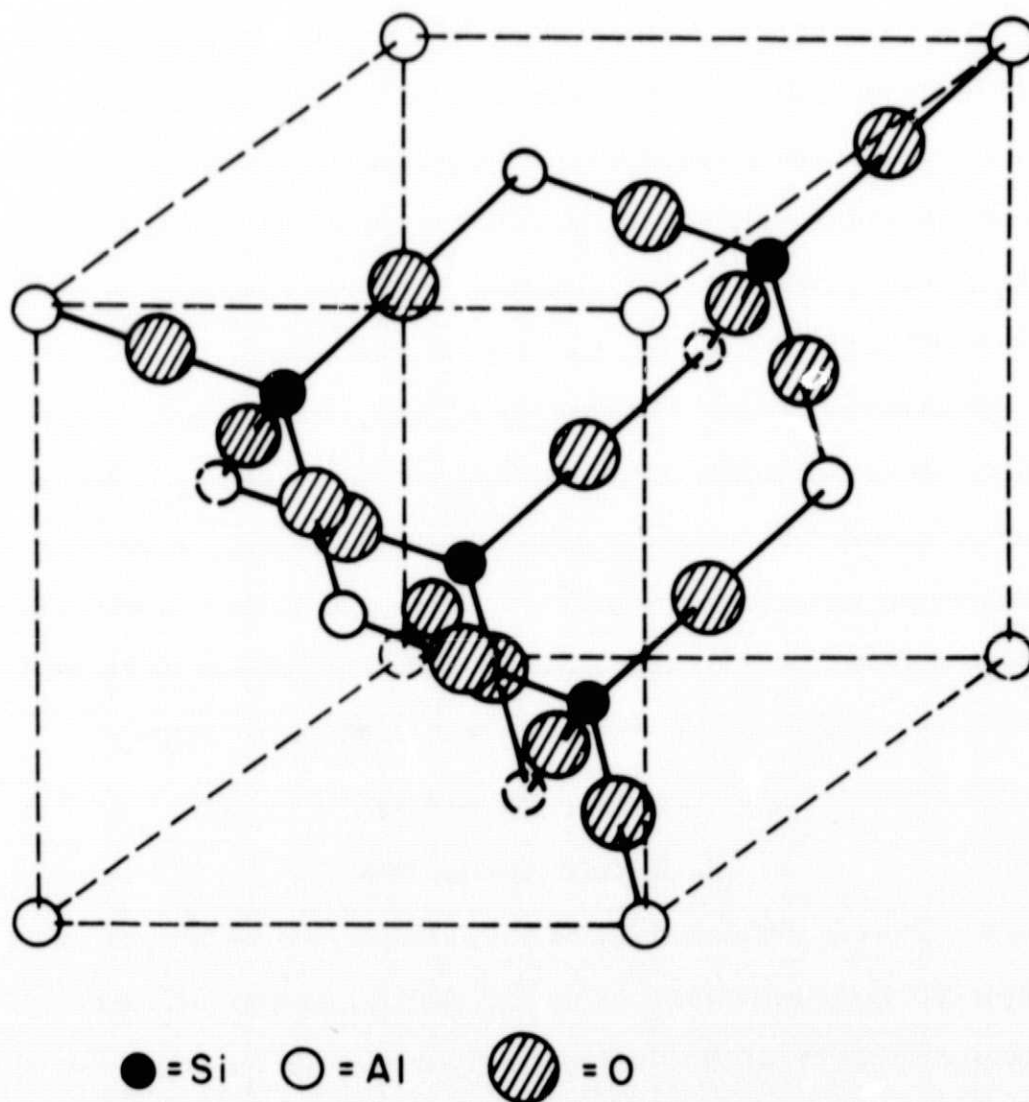
7

● = Si   ◯ = Al   � = O

Fig. 4. The AlSiO$_4$ subarray of carnegieite.

2. Chemical stability. To prevent a material from being either oxidized or reduced, it may be necessary to use special dies and pistons as well as a controlled atmosphere.

3. Phase stability. Some idea of the T-P phase diagram for a material is important. At the extreme conditions used in hot pressing, phase transformations are common. This is especially true of many of the metastable phases considered in this investigation. Lack of thermal stability may call for high pressures for densification, and high pressures may promote phase transformation.

4. Particle size. Some materials resist high densification unless the initial particle size is very small ($< 1 \mu m$).

We have developed three hot-pressing stations capable of operating to about $1200^{\circ}C$. One of these is a vacuum or controlled-atmosphere station. These systems employ dies and pistons of various types; ceramic, graphite, steel, tungsten carbide. We also employed hydrostatic-pressure equipment capable of performing a sample and binder to 30,000 atmospheres and subsequently firing to $1700^{\circ}C$.

B. Powder Preparation

Powder samples of stable phases were prepared by conventional methods.

Metastable phases were prepared either by high-pressure synthesis or by ion exchange in molten nitrates.

IV. TRANSPORT MEASUREMENTS

A. Ionic Conductivity

Ionic conductivity was generally measured on ceramic disks with an ac vector-impedance meter (5Hz to 500 kHz) and the use of both blocking and non-blocking electrodes. The blocking electrodes permit electron transport, but restrict ion transport to a displacement current. The non-blocking electrodes consist of a coating of colloidal graphite on both sides of the sample. Because Na^+ ions can be discharged into such electrodes, polarization is avoided at higher frequencies and is often trivial

even at frequencies as low as 500 Hz. In the lower resistance ranges, the impedance meter applies a sinusoidal potential of about 2.7 m V rms and yields a simultaneous readout of impedance and phase angle.

For comparison purposes, some dc and low-frequency ac measurements were made with molten $NaNO_3$ on both sides of the specimen. These molten-salt measurements have been in good agreement with data obtained with the "reversible" graphite electrodes. Of course, the only truly reversible electrodes would be molten sodium. However, interface problems make the sodium electrodes less useful in normal evaluation studies. The graphite electrodes are useful because, while not reversible, they are "non-polarizing". Specimens were also forwarded to Dr. Joseph Singer of NASA Lewis for independent evaluation.

B. Voltage Pulse with Blocking Electrodes

In order to investigate the ionic conductivity in more detail, we devised an unconventional measurement procedure.

The experimental arrangement is shown in Fig. 5. The sample is placed between two copper electrodes, but separated from them by sheets of gold that serve as blocking electrodes. Our early measurements were plagued by a lack of reproducibility resulting primarily from diffusion of copper from the electrodes through the 0.0001-in. gold blocking sheets and into the samples. The quality of our recent data was greatly improved by the use of self-aligning copper electrodes together with 0.01-in. gold sheets for blocking. Trains of pulses of alternating polarity (to avoid permanent polarization of the sample) separated by quiescent intervals are applied to the electrodes. The pulse risetime is approximately 100 nanoseconds, the amplitude can be varied from 0.1 to 10 volts, the pulse width from 1 millisecond to 5000 seconds, and the duty cycle from 12 to 100%. The resulting current i(t) that flows in the external circuit is first preamplified, then sampled by a gated amplifier, compressed by a logarithmic converter, and finally plotted as a function of time on an X-Y recorder.

10
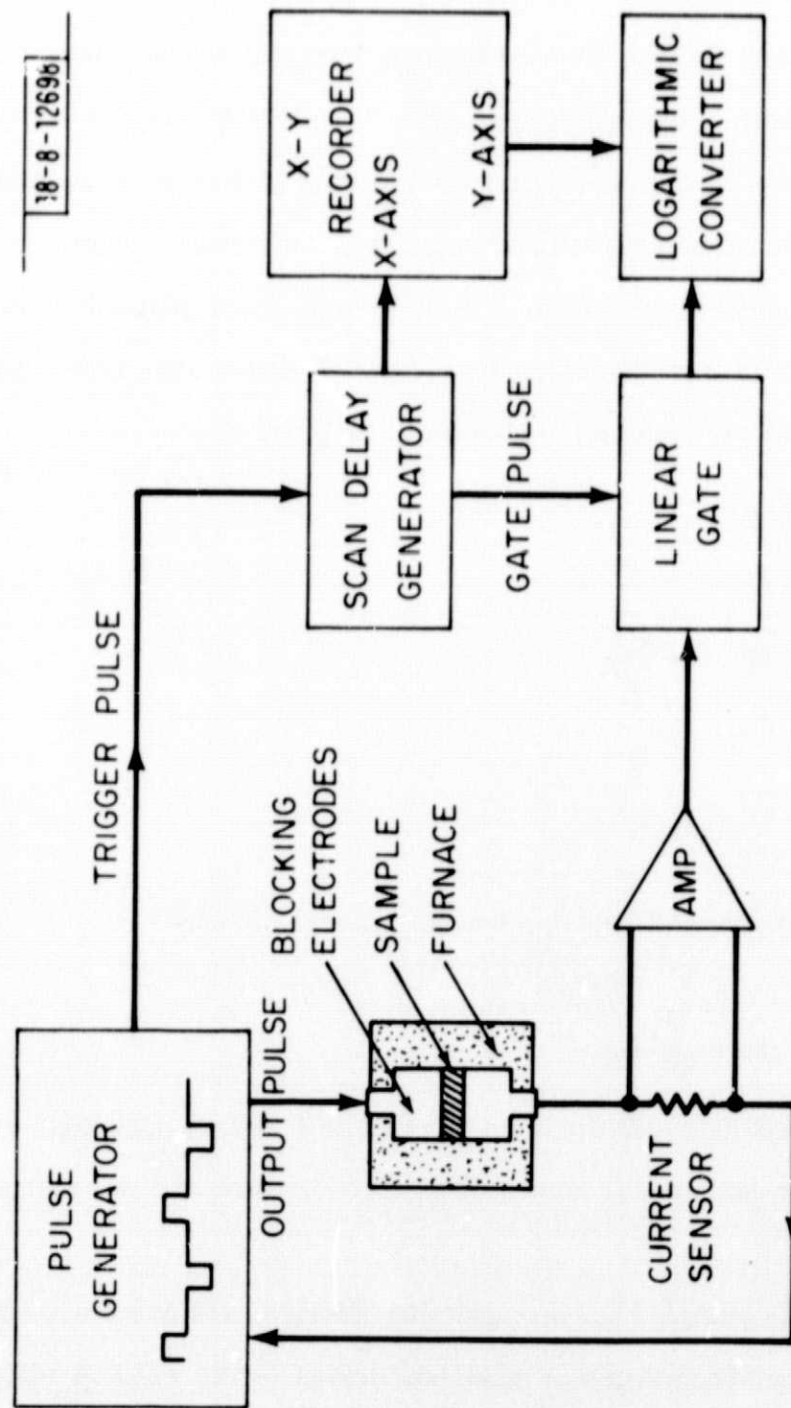
Fig. 5.   Experimental arrangement for measuring current response to a voltage

pulse with blocking electrodes.

11

Samples were tested for the presence of electron mobility by the application of wide pulses. All ionic current must eventually decay to zero, since the ions cannot pass through the blocking gold electrodes, whereas electron current will persist. This measurement showed one sample of $NaTa_2O_5F$ to possess approximately 1% electronic conduction at $300^{\circ}C$. No electronic contribution to the conductivity was found in any other sample, our limit of sensitivity being of the order of 0.03%.

Given purely ionic conductivity, the blocking electrodes must behave like capacitors. If the electrolyte behaved like a resistor, then the graph of log i(t) vs time would be a straight line, whereas our results are curved over all time ranges. However, if we treat the electrolyte as a resistor R in series with a varying capacitance $C_{eff}(t)$, then the potential drop is initially given by

$$V = R \, i(0) \, , \tag{1}$$

and subsequently by

$$V = R \, i(t) + \frac{Q(t)}{C_{eff}(t)} \, , \tag{2}$$

where

$$Q(t) = \int_0^t i(t')\,dt' \, . \tag{3}$$

Since the applied potential remains constant during the pulse,

$$R \, C_{eff}(t) = \frac{\int_0^t i(t')\,dt'}{i(0) - i(t)} \, . \tag{4}$$

We have calculated this quantity from our data and find its logarithm to increase approximately linearly in log time over several decades of time, with a slope close to 0.5.

All ceramic samples possess grain boundaries, and hence are not truly homogeneous. Charge accumulates at these boundaries, which act like additional capacitors in series with the contact capacitance C between the blocking electrodes and the sample. As charge leaks across the grain boundaries, their share of the potential

12

drop decreases, which constitutes an increase in $C_{eff}(t)$. Our problem is to be able to calculate this increase on the basis of some model of the material, or more precisely, some model of the grain boundaries in the material.

The simplest equivalent circuit for a ceramic electrolyte with reversible electrodes consists of a bulk resistance R in series with the parallel combination of a capacitance C_b and resistance R_b arising from the grain boundaries (see Fig. 6). The neglect of parallel paths through neighboring grains requires that the boundary impedance be high compared to the interior resistance. Recent measurements by Powers and Mitoff[7] show that this condition is satisfied in the case of β-alumina. They find the transition region from low-frequency to high-frequency impedance $Z(\omega)$ to be somewhat broader than calculated from the equivalent circuit, but give the plausible rationale that one should expect a distribution of grain-boundary impedances.

If blocking electrodes are used, the corresponding equivalent circuit includes an additional contact capacitance C in series with the internal resistance R. The current vs time response of such a circuit to an applied voltage step consists of two regions of exponential decay joined by a brief transition interval. Thus the graph of log I vs time consists of two straight lines, and the curved transition region appears brief indeed on a time scale that extends over six orders of magnitude from 100 ns to 100 ms. The decay of its current response to a pulse is a more distinctive characteristic of the circuit than the frequency dependence of its impedance.

In contrast to such theoretical behavior, our measurements on samples of various materials (e.g. $NaSbO_3 \cdot (1/6)NaF$, $NaTa_2O_5F$, $Na_2Al_{22}O_{34}$) all show a smooth, sweeping curvature in the graph of log I vs time over this entire range of time, and even beyond. Therefore, the simple explanation of this observed shape in terms of a reasonable distribution of grain-boundary impedances is not plausible, and we are forced to re-examine the basic mechanisms of ionic conduction.
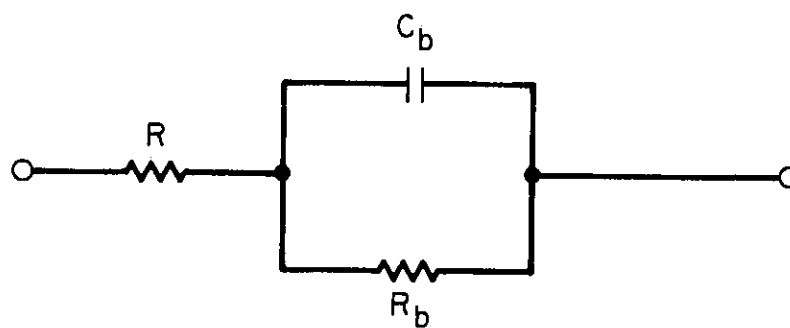
13

Fig. 6.   Simplest equivalent circuit for a ceramic electrolyte.

Let $p(x, t)$ denote the concentration of mobile charge, $i(x, t)$ the current density, and $E(x, t)$ the electric field. Then the distribution of ions inside a continuous medium is to be found by solving the differential equation:

$$\frac{\partial}{\partial t} p(x, t) = -\frac{\partial}{\partial x} i(x, t) = -\frac{\partial}{\partial x} \left[\mu(x)p(x, t)E(x, t) - D(x) \frac{\partial}{\partial x} p(x, t) \right] , \qquad (5)$$

where $\mu(x)$ and $D(x)$ are the mobility and diffusion constant, respectively. A grain boundary is a narrow region in which the mobility μ_b differs from μ in the bulk material. In fast ion conductors, μ_b is much smaller than μ, so that a surplus of carriers piles up on one side of the boundary region, while a deficiency arises on the other. This condition creates a large concentration gradient across a grain boundary. Equilibrium is not attained until the carriers find their way through the boundary region. Since the diffusion term is non-ohmic, no equivalent circuit can be a valid representation of Eq. (5) unless $D \, \partial p / \partial x$ is negligible for all x and all t.

In our most recent pulse experiments, we have measured the decay of the discharge current as well as that of the charging current. The two decays must be identical for any ohmic equivalent circuit (unless electronic current shunts the contact capacitance, in which case the total amounts of transported charge will differ). We find a difference in the decay curves, but with the same total charge transferred during discharge as during the charging cycle, which indicates the presence of a diffusion current. The discharge current is greater than the charging current initially, but then decays faster, in agreement with the predicted behavior of a diffusion contribution from the bulk. Conventional a.c. techniques would have been unable to demonstrate this presence of a diffusion contribution to the current.

Since the mobility is lower at grain boundaries, we can expect the diffusion term to be even more important there than in the bulk. We conclude that the curvature of the graph of log I vs time is in large part due to the discharge of C_b by a predominantly diffusive current. Thus comparison between experiment and solutions of Eq. (5)

15

can yield important insight into the character of grain boundaries in ceramic electrolytes.

V. RESULTS

A. Antimonates

1. NaSbO$_3$. An isomorphous, metastable "NaSbO$_3$" phase having the cubic Im3 structure was obtained by ion exchange, the high-pressure Im3 phase of KSbO$_3$ or of TlSbO$_3$ being immersed for a few hours in molten NaNO$_3$. Single-crystal structure analysis, [8] obtained by ion exchange of a crystal of TlSbO$_3$, located the Na$^+$ ions randomly distributed among the octahedral M$_1$ and M$_2$ sites of Fig. 2. This analysis produced three significant findings:

(1) The apparent sodium concentration is in excess of stoichiometry, suggesting a chemical formula Na$_{1+x}$SbO$_3$ with $x \approx 0.29$.

(2) There is no electron density in the tunnel intersections at the origin and body-center positions.

(3) In the disordered Im3 phase, Na$^+$-Na$^+$ separations of only 2.303 Å must occur, especially as the occupancy factors of the M$_1$ and M$_2$ sites were in the ratio 0.82/0.29 rather than 2/1.

In the absence of detailed chemical analysis, the apparent excess sodium obtained by x-ray analysis could be at least partially due to an incomplete exchange of the heavier Tl$^+$ ions by Na$^+$ ions. In our early work, we used only a single ion-exchange bath.

High pressure stabilizes the cubic Im3 phase of KSbO$_3$ because this phase is more dense than the ilmenite phase. For NaSbO$_3$, the situation is reversed, which limits the pressure that can be applied for densification of the metastable, cubic NaSbO$_3$. Because it is metastable, the temperature that can be used for densification is also limited. Nevertheless, we were able to obtain specimens of 92-98 percent theoretical density by using a NaNH$_2$ fluxing agent. A mixture of fine (< 1 μm) powder

16

and 2 weight percent $NaNH_2$ was placed in a tungsten-carbide die-and-piston assembly. The system was evacuated to pressures less than 1 μm. A pressure of 30,000 psi was applied, the temperature was raised to $600^{o}C$ and held for an hour or so; the pressure was then released and the specimen allowed to cool. After removal, the specimen was baked out in a vacuum at $500^{o}C$.

Conductivity measurements showed no measurable electronic contribution and an ionic resistivity at $300^{o}C$ of ρ_{300} = 18 Ω-cm at 1000 Hz with graphite electrodes. The fact that this resistivity is only a factor of four larger than that of the best β''-alumina samples at $300^{o}C$ demonstrates the validity of the skeleton-structure concept.

2. $\underline{NaSbO_3 \cdot \frac{1}{6} NaF}$. Since the tunnel-intersection sites are empty in $NaSbO_3$, it suggests that they repel positive ions. If so, the Na^+ ions jump from M_1 site to M_1 site without passing through the tunnel intersections. This would mean that placement of an anion at the intersection sites could stabilize the cubic $KSbO_3$ structure, thus explaining Spiegelberg's stabilization of the Pn3 phase of $KSbO_3$ by annealing for three weeks at $1000^{o}C$ in a porcelain crucible, without interfering with the Na^+-ion transport.

A telephone communication from R. S. Roth of NBS, which suggested that anion substitutions might stabilize $KSbO_3$ at atmospheric pressure, led us to investigate $KSbO_3 \cdot \frac{1}{6} KF$. Roth independently tried stabilization of $KSbO_3$ by fluorine substitutions, and reported[9] the atmospheric-pressure preparation of $K_{1-x}SbO_{3-x}F_x$. Since he failed to report any chemical analysis, it is probable that his phase was also $KSbO_3 \cdot \frac{1}{6} KF$. We were interested not only in the possibility, first recognized by Roth, of eliminating a high-pressure step in the preparation of $NaSbO_3 \cdot \frac{1}{6} NaF$, but also in whether the existence of an anion at the tunnel intersections would aid or hinder Na^+-ion mobility.

The precursor $KSbO_3 \cdot \frac{1}{6} KF$ was prepared by firing a 2:1 weight ratio of $K_2H_2Sb_2O_7 \cdot 4H_2O$ and KF at $900^{o}C$ for 2 hours. Subsequent leaching of the product removed the excess KF, leaving the compound $KSbO_3 \cdot \frac{1}{6} KF$. This compound was immersed in molten $NaNO_3$ at $325^{o}C$ for 2 hours and then water leached. Three such

17

treatments yielded a pure product, identified by both chemical and structural analysis[10] as $NaSbO_3 \cdot \frac{1}{6}NaF$. The F^- ions occupy the tunnel intersection sites of the Im3 structure, and the Na^+ ions are randomly distributed on the octahedral M_1 and M_2 sites. The shortest Na-Na distance, between M_1 sites of neighboring tunnels, is here 2.87 Å.

Although $NaSbO_3 \cdot \frac{1}{6}NaF$ has moderate temperature stability, it cannot be heated to temperatures near the melting point. Therefore, high pressures are required for densification. However, at 5000 atmospheres and $600^{\circ}C$, there is partial disproportionation and transformation to the more dense ilmenite phase of $NaSbO_3$. Consequently, the densification procedures used for $NaSbO_3$ specimens were also employed for $NaSbO_3 \cdot \frac{1}{6}NaF$ samples.

Figure 7 shows a plot of resistance vs 1/T for a typical specimen of $NaSbO_3 \cdot \frac{1}{6}NaF$. The slope yields an activation energy of ~ 0.35 eV for a Na^+-ion jump. This is about a factor 2 larger than that found for β-alumina. However, the pre-exponential factor is smaller, which means that $NaSbO_3 \cdot \frac{1}{6}NaF$ has a smaller resistivity than β-alumina at higher temperatures. The difference in pre-exponential factors reflects, presumably, the fact that the entire volume of $NaSbO_3 \cdot \frac{1}{6}NaF$ participates in Na^+-ion conduction. Comparison of three different measurement techniques gave $\rho_{300} = 13$, 17 and 18 Ω-cm, respectively, for graphite electrodes and 1000 Hz, molten $NaNO_3$ electrodes and 1000 Hz, and molten $NaNO_3$ with d.c.

From Fig. 7 we deduce three conclusions: (1) cubic skeleton structures have the improvement in pre-exponential factor anticipated for bulk vs layer Na^+-ion conduction, (2) placement of an anion at the tunnel intersections does not impede the Na^+-ion mobility, thereby confirming that the Na^+ ions avoid these positions in $NaSbO_3$, and (3) reduction in the Na^+-ion activation energy ϵ_a for hopping, which might be achieved, for example, were occupancy of the M_1 and M_2 sites equivalent, could make the transport properties of cubic skeleton structures superior to those of β-alumina.
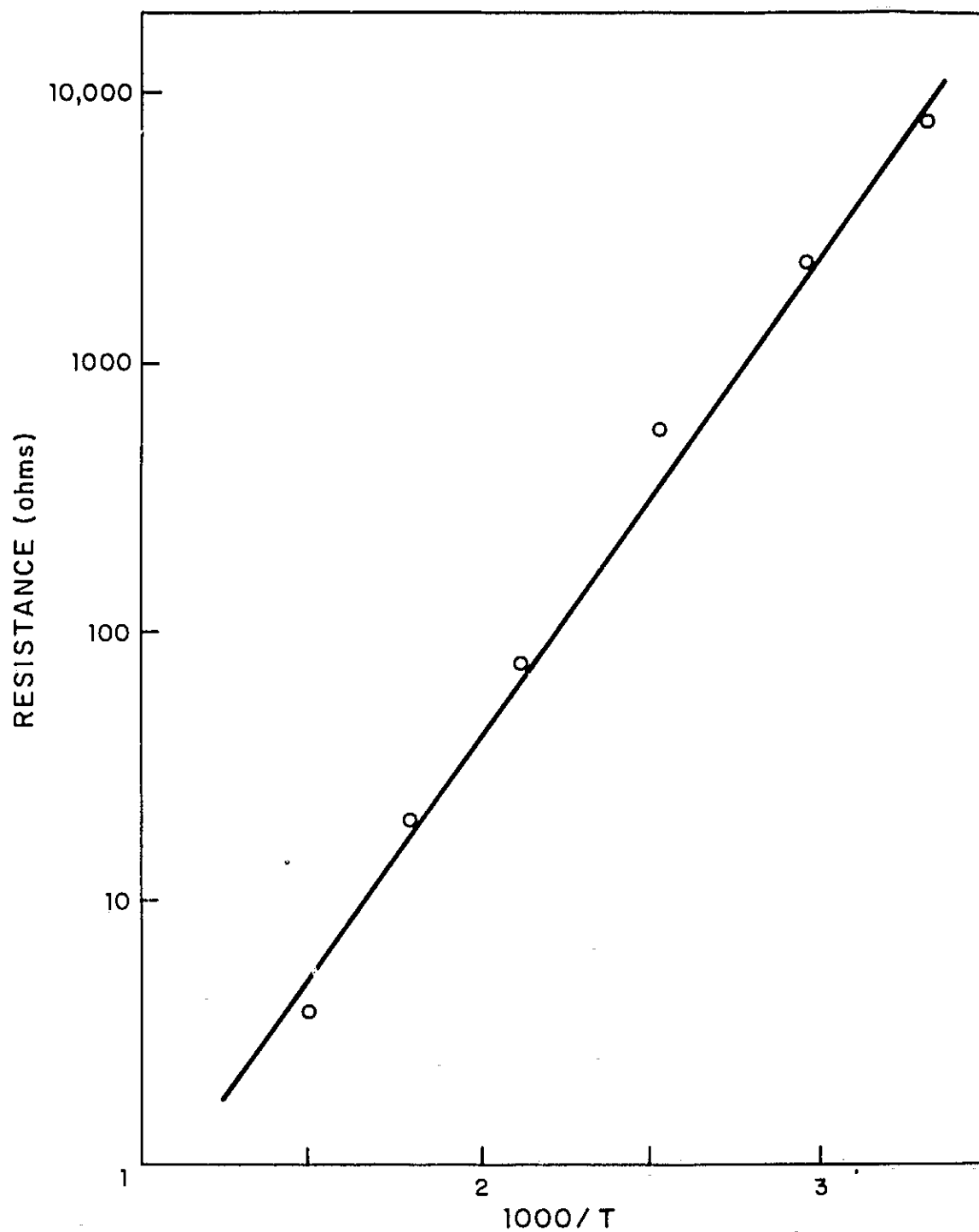
Fig. 7. Resistance vs 1/T for a typical specimen of $NaSbO_3 \cdot \frac{1}{6}NaF$.

In order to determine whether ϵ_a would be decreased by lattice contraction, we studied the conductivity as a function of pressure. Unfortunately, the die broke before we could obtain a quantitative set of data. However, the measurements clearly indicated that the conductivity decreased with the lattice parameter. Therefore, we conclude that a smaller ϵ_a can be achieved by increasing the lattice parameter. An earlier study of $KBiO_3$ indicated that this compound, thought it has the same structure, is hygroscopic. It would be interesting to explore the system $NaSb_{1-x}Bi_xO_3 \cdot \frac{1}{6}NaF$ to see how the ionic conductivity changes with increasing cell size.

B. Pyrochlores

Initially, we prepared the defect-pyrochlore $KTaWO_6$ by conventional ceramic techniques. A nominal $NaTaWO_6$ was prepared by ion exchange in molten $NaNO_3$. At $300^\circ C$, the resistivity of this compound was about a factor 10 larger than that of $NaSbO_3 \cdot \frac{1}{6}NaF$, but a lower activation energy made it interesting. Because W^{6+} ions would be reduced to W^{5+} ions by molten sodium, we turned to a study of the chemically more stable pyrochlore $A^+Ta_2O_5F$. In this study[11] we found that the pyrochlores may be hydrated, and a subsequent investigation of nominal $NaTaWO_6$ showed it to be, in fact, partially hydrated: $NaTaWO_6 \cdot xH_2O$ with $x \approx 0.5$.

The compound $RbTa_2O_5F$ can be synthesized directly. Equal amounts of dry RbF and reagent-grade Ta_2O_5 were mixed in a crucible and fired at $750^\circ C$ under an argon atmosphere for two days. Regrinding and refiring two times produced single-phase powders. Single crystals of $RbTa_2O_5F$ were prepared by addition of excess RbF as a flux. In one run, a 4:1 molar ratio of RbF and Ta_2O_5 was fired at $1150^\circ C$ for 30 minutes and quenched. The product contained crystals about 0.1 mm across.

The K and Na analogs could not be synthesized directly. If $RbTa_2O_5F$ is placed in molten KNO_3, the product of ion exchange is KTa_2O_5F. However, on exposure to air it becomes hydrated to $KTa_2O_5F \cdot H_2O$. The lattice parameter of $RbTa_2O_5F$ is 10.496 Å, of $KTa_2O_5F \cdot H_2O$ is 10.605 Å. TGA measurements showed a reversible, broad transition, from 50° to $200^\circ C$, having a weight loss of one H_2O molecule per

20

KTa_2O_5F molecule. Although our measurements on powder samples showed an amorphous dehydration product, a repeat of our experiment by R. S. Roth of NBS gave a cubic lattice parameter $a = 10.49$ Å, somewhat smaller than that of the hydrated compound but anomalously large relative to the parameter for $RbTa_2O_5F$. This finding suggests that the K^+ ions are not restricted to the large 8b sites, as are the Rb^+ ions, but occupy -- at least partially -- the 16d positions. A single-crystal x-ray study of $KTa_2O_5F \cdot H_2O$ revealed electron density of both the 16d and 8b sites in a ratio 2.5:1, and it was not possible to distinguish whether the water on the K^+ ions occupied the 8b positions preferentially.

Attempts to prepare $NaTa_2O_5F$ by ion exchange of $RbTa_2O_5F$ in molten $NaNO_3$ yielded incompletely exchanged products. However, ion exchange first with K^+ ions and then with Na^+ ions did yield a completely exchanged product. Although chemical analysis gave a Rb:Ta and a K:Ta ratio of 1:2, as anticipated, the Na:Ta ratio is x:2, where $x \approx 2$. These same Rb:Ta and K:Ta ratios were obtained on reversing the ion exchange. Moreover, structural analysis gave an apparent Na^+-ion excess equivalent to $x \approx 3$. We thought this discrepancy might be due to the presence of OH^- ions, giving $Na_2Ta_2O_5F \cdot OH$, but neither IR data nor TGA experiments nor the preparation of "$NaTa_2O_5F$" from anhydrous KTa_2O_5F gave any evidence of the presence of OH^- ions. Since electrical measurements gave no measurable electronic component, the excess sodium appears to be charge compensated by some anion -- presumably O^{2-} ions.

Anion analysis (by vacuum fusion at MIT) of "$Na_{1-x}Ta_2O_5F$" for a sample with $x = 0.55$ gave $Na_{1.55}Ta_2O_5F \cdot O_{0.28}$, which provides direct evidence that the excess Na^+ ions are charge-compensated by additional O^{2-} ions, which presumably occupy the 8b positions. It is probable that the excess Na^+ ions in $(Na_2O)_{1+x} \cdot 11Al_2O_3$ and any excess Na^+ ion in $NaSbO_3$ are also charge-compensated by additional O^{2-} ions.

Preparation of hot-pressed, ceramic disks is complicated by the fact that both pressure and temperature induce disproportionation to the perovskite $NaTaO_3$ and

21

TaO_2F. Specimens approaching 82 percent theoretical density were prepared by the same procedures used to obtain pellets of $NaSbO_3$. A $\rho_{300} \approx 150$ Ω-cm and an $\varepsilon_a \approx 0.4$ eV were obtained with graphite electrodes and 1000 Hz.

Examination of the defect-pyrochlore fluorides prepared by Babel et al.[5] reveals that the Rb and Cs compounds, which have A^+ ions only in 8b sites, are dehydrated. The K compounds, on the other hand, are only dehydrated if the lattice parameter is small enough to retain the K^+ ions in 8b sites ($KNiAlF_6$ with a = 9.92 Å). Compounds with larger lattice parameters are hydrated: $KNiCoF_6$ has a = 10.18 Å and $KNiCoF_6 \cdot H_2O$ has a = 10.45 Å, $KCoCrF_6 \cdot H_2O$ and $KNiVF_6 \cdot H_2O$ are only reported with the hydrated parameters a = 10.48 and 10.51 Å. These findings suggest that there may be a critical lattice parameter for hydration as well as one at which the K^+ ion has the same preference for 8b and 16d sites.

Ion exchange of $RbMgAlF_6$, a = 9.94 Å, gives dehydrated $KMgAlF_6$ with a = 9.86 Å and a non-cubic "$NaMgAlF_6$", which can be reverse ion exchanged. The ion conductivity of $KMgAlF_6$ is extremely low. We suspected this low conductivity reflected a filled 8b array. In this case, transfer of a K^+ ion to a neighboring 16d position costs a large K^+-K^+ electrostatic energy, since each 16d position has two near-neighbor 8b positions at a distance of only 2.12 Å. In order to test this reasoning, we prepared samples with chemical formula $K_{1-x}Mg_{1-x}Al_{1+x}F_6$, x = 0.05 and 0.10. The introduction of cation vacancies at 8b positions should permit K^+-ion transport from one 8b site to another via the 16d intermediary position. A dramatic increase in conductivity was observed. A plot of K^+-ion conductivity vs reciprocal temperature for a $K_{0.9}Mg_{0.9}Al_{1.1}F_6$ disk over 99 percent dense gave $\rho_{300} \approx 800$ Ω-cm and an $\varepsilon_a \approx 0.35$ eV, which is to be compared with 0.284 eV in β-alumina.

From these experiments we may draw the following conclusions: (1) The B_2X_6 network of the $A_2B_2X_6X'$ pyrochlore structure is a suitable skeleton for fast ion transport. (2) Direct preparation of defect pyrochlores $A^+B_2X_6$ requires large A^+ cations (Cs^+, Rb^+, and -- for lattice parameters below a critical size -- K^+ ions) that are

22

stabilized in the 8b (or X') positions. (3) Fast ion transport of K^+ ions among 8b sites requires the introduction of 8b-site vacancies, as in $K_{0.9}Mg_{0.9}Al_{1.1}F_6$. (4) Indirect preparation of detect pyrochlores $A^+B_2X_6$ having smaller A^+ cations randomly distributed on 16d sites is plagued by the introduction of water or of anions on the 8b sites. We were unable to obtain a "clean" $A^+B_2X_6$ pyrochlore having A^+ ions on the 16d positions. However, Na^+-ion transport in partially filled 16d positions occurs in $Na_{1+2x}Ta_2O_5F \cdot O_x$.

In order to determine whether the Na^+ ions travel only on 16d positions, or jump via 8b sites, it would be useful to prepare $NaTa_2O_4F_2 \cdot F$. Unfortunately we had difficulty obtaining the TaO_2F starting material during this contract period.

C. Aluminosilicates

Although the contract did not specify work on the aluminosilicates, some preliminary work was done. Because cubic $NaAlSiO_4$ is unstable at room temperature, the related stable compounds $Na_4Al_2Si_2O_9$ and $Na_3Al_2Si_2O_{8.5}$ were prepared. These have the $NaAlSiO_4$ structure of carnegiete, but with excess Na_2O. The position of the excess O^{2-} ions has not been determined. Transport measurements on disks of ca 75 percent density gave a $\rho_{300} \approx 110$ Ω-cm and 1900 Ω-cm, respectively, for the two compounds with graphite electrodes and 1000 Hz.

23

References

1. Y. F. Yao and J. T. Kummer, J. Inorg. Nucl. Chem. $\underline{29}$, 2453 (1967).

2. R. Ridgeway, A. Klein, and W. O'Leary, Trans. Electrochem. Soc. $\underline{70}$, 71 (1936).

3. P. Spiegelberg, Ark. Kemi $\underline{14A}$, 1 (1940).

4. J. A. Kafalas, Solid State Chemistry, Proc. 5th Materials Res. Symp. Inst. Materials Res., NBS Oct. 18-21, 1971, R. S. Roth and S. J. Schneider, Jr. eds. (U.S. Dept. Commerce, 1972) p. 287; J. B. Goodenough and J. A. Kafalas, J. Solid State Chem. $\underline{6}$, 493 (1973).

5. D. Babel, G. Pausewang, and W. Viebahn, Z. Naturforsch. $\underline{22b}$, 1219 (1967).

6. J. Singer, private communication.

7. R. W. Powers and S. P. Mitoff, J. Electrochem. Soc. $\underline{122}$, 226 (1975).

8. H. Y-P. Hong, J. A. Kafalas, and J. B. Goodenough, J. Solid State Chem. $\underline{9}$, 345 (1974).

9. W. S. Brower, D. B. Minor, H. S. Parker, R. S. Roth, and J. L. Waring, Mater. Res. Bull. $\underline{9}$, 1045 (1974).

10. H. Y-P. Hong, J. A. Kafalas, J. B. Goodenough, C. H. Anderson, Jr., and D. M. Tracy, Lincoln Laboratory, MIT, Solid State Research Report (1974:2), p. 20.

11. J. B. Goodenough, H. Y-P. Hong, and J. A. Kafalas, Lincoln Laboratory, MIT, Solid State Research Report (1974:3), p. 32.

BIBLIOGRAPHIC DATA SHEET	1. Report No. NASA/C-43205-C/FR/75	2.	3. Recipient's Accession No.

4. Title and Subtitle		5. Report Date prepared March 31, 1975
Research for Preparation of Cation-Conducting Solids by High-Pressure Synthesis and Other Methods		6.

7. Author(s) J. B. Goodenough, H. Y-P Hong, J. A. Kafalas, K. Dwight, Jr.	8. Performing Organization Rept. No.

9. Performing Organization Name and Address	10. Project/Task/Work Unit No.
MIT Lincoln Laboratory Lexington, Ma. 02173 (P.O. Box 73)	11. Contract/Grant No. NASA Contract C-43205-C

12. Sponsoring Organization Name and Address	13. Type of Report & Period Covered Final Report 1 Aug. 1973-28 Feb. 1975
NASA-Lewis Research Center 21000 Brookpark Road Cleveland, Ohio 44135	14.

15. Supplementary Notes

16. Abstracts

Fast Na^+-ion transport has been demonstrated for two body-centered-cubic skeleton structures. A resistivity at $300^\circ C$ of $\rho_{300} \approx 12$ Ω-cm and an $\epsilon_a \simeq 0.35$ eV show that the conductivity is competitive or superior to β''-alumina above $400^\circ C$, but is inferior below. The activation energies are a factor two higher than in β''-alumina. Comparison of the Na^+-ion conductivity of $NaSbO_3$ and $NaSbO_3 \cdot (1/6)NaF$ showed that Na^+-ion transport is not impeded by placement of F^- ions at the tunnel intersections. Conductivity of K^+ ions in the defect pyrochlore $KMgAlF_6$ was greatly improved by introducing K^+-ion vacancies: $K_{1-x}Mg_{1-x}Al_{1+x}F_6$. Potassium pyrochlores with cell size greater than a critical value became hydrated in air, as exemplified by $KTa_2O_5F \cdot H_2O$. The sodium analogue is dehydrated, but always contains extra Na_2O to give $Na_{1+2x}Ta_2O_5F \cdot O_x$.

17. Key Words and Document Analysis.   17a. Descriptors

Solid Electrolytes

Na^+-Ion Transport

Sodium-Sulfur Battery

17b. Identifiers/Open-Ended Terms

Electrical Storage in Secondary, High-Specific-Energy Batteries

Fast Na^+-Ion Transport in Ceramic Membranes

17c. COSATI Field Group

18. Availability Statement	19. Security Class (This Report) UNCLASSIFIED	21. No. of Pages 30
Unclassified - unlimited	20. Security Class (This Page) UNCLASSIFIED	22. Price